

Journal of Biomedical Optics

BiomedicalOptics.SPIEDigitalLibrary.org

Taking advantage of hyperspectral imaging classification of urinary stones against conventional infrared spectroscopy

Francisco Blanco
Felipe Lumbreras
Joan Serrat
Roswitha Siener
Silvia Serranti
Giuseppe Bonifazi
Montserrat López-Mesas
Manuel Valiente

Taking advantage of hyperspectral imaging classification of urinary stones against conventional infrared spectroscopy

Francisco Blanco,^a Felipe Lumbreras,^b Joan Serrat,^b Roswitha Siener,^c Silvia Serranti,^d Giuseppe Bonifazi,^d Montserrat López-Mesas,^{a,*} and Manuel Valiente^a

^aUniversitat Autònoma de Barcelona, Centre Grup de Tècniques de Separació en Química (GTS), Unitat de Química Analítica, Departament de Química, 08193 Bellaterra, Spain

^bUniversitat Autònoma de Barcelona, Computer Vision Center & Department of Computer Science, 08193 Bellaterra, Spain

^cUniversity Stone Centre, Department of Urology, University of Bonn, Sigmund-Freud-Str. 25, 53105 Bonn, Germany

^dSapienza-Università di Roma, Dipartimento di Ingegneria Chimica Materiali Ambiente (DICMA), 00184 Roma, Italy

Abstract. The analysis of urinary stones is mandatory for the best management of the disease after the stone passage in order to prevent further stone episodes. Thus the use of an appropriate methodology for an individualized stone analysis becomes a key factor for giving the patient the most suitable treatment. A recently developed hyperspectral imaging methodology, based on pixel-to-pixel analysis of near-infrared spectral images, is compared to the reference technique in stone analysis, infrared (IR) spectroscopy. The developed classification model yields >90% correct classification rate when compared to IR and is able to precisely locate stone components within the structure of the stone with a 15 μm resolution. Due to the little sample pretreatment, low analysis time, good performance of the model, and the automation of the measurements, they become analyst independent; this methodology can be considered to become a routine analysis for clinical laboratories.

© 2014 Society of Photo-Optical Instrumentation Engineers (SPIE) [DOI: [10.1117/1.JBO.19.12.126004](https://doi.org/10.1117/1.JBO.19.12.126004)]

Keywords: kidney stone; urinary stone analysis; urinary stones classification; hyperspectral imaging; infrared spectroscopy; near-infrared.

Paper 140394RR received Jun. 24, 2014; accepted for publication Oct. 24, 2014; published online Dec. 5, 2014.

1 Introduction

The prevalence and incidence of stone disease, which affects up to 12% of the population in developed countries, is increasing worldwide.^{1,2} Therefore, an accurate description of the causes of the disease is of major importance for the definition of the risk profile of the patient. The metabolic disturbances experienced by the patient and lifestyle factors are strongly related to the type and composition of the resulting stone.^{3,4} Hence, this information stands as a key diagnosis to determine the most suitable treatment for each patient and reduce the high recurrence rate. A better description of the underlying mechanisms could improve the patient's quality of life and strongly reduce the important medical costs linked to urinary stones management.^{5,6}

The simplicity of the sample treatment, the low cost associated with the measurements, and the usefulness of the obtained results have led infrared (IR) spectroscopy to become the reference method as well as the most widely used technique for urinary stones characterization.⁷ In addition, some quantification methodologies based on IR spectroscopy have also been developed. In this regard, the most relevant bibliography describes linear quantification models based on the calculation of the ratio of single spectral bands (specific for each type of urinary stone), so most of the information on the spectra is not used into the calculations.^{8,9} Despite the popularity of IR analysis, it also shows some limitations derived from the sample treatment. Due to the need of grinding the sample for its analysis either to

prepare a pellet or by using attenuated total reflectance (ATR), the spatial dimension of the determination is lost.

The traditional alternative to IR for a space-defined characterization of the stone is the optical microscopy approach,¹⁰ which is usually linked to elemental analysis. A correct interpretation of the results obtained by this methodology can bond the stone to the different etiologic situations the patient has gone through. The high detail of the results, though, is strongly dependent on the analyst's expertise and is also time-consuming. Besides, this approach is not cost-effective for widespread use in general clinical laboratory.

Despite its restrictions, the use of microscopy has allowed the establishment of a correlation of the stone structure with the etiological factors that led to its formation, which has been properly addressed in bibliography.¹⁰⁻¹² Other high-resolution imaging approaches have also indicated the relevance of a proper description of the component distribution.¹³ As an example, the location of carbonate apatite only in the core of calcium oxalate stones suggests the existence of a Randall plaque, a direct result of renal tissue damage, which requires specific treatment. Such degree of detail is efficiently achieved using imaging techniques.¹⁴ Nowadays, hyperspectral imaging (HSI) techniques are becoming the trend for diagnosis in many medical fields and have been often applied to tissue analysis.¹⁵ HSI allows the analysis of large datasets by the use of multivariate analysis techniques.¹⁶ They have also been implemented for the analysis of urinary stones by Pucetaite et al.¹⁷ and Piqueras et al.¹⁸ The former experiment included a descriptive pixel-to-pixel

*Address all correspondence to: Montserrat López-Mesas, E-mail: monserrat.lopez.mesas@uab.cat

analysis of only a few urinary stones, and at a lower resolution compared with the work described here. The latter uses high-precision equipment that yields excellent resolution results and implements a chemometric model for the classification of pixels. However, the measurement of the suggested IR maps requires, naturally, a significant amount of time to be performed.

In a previous work, a novel methodology based on HSI was developed.¹⁹ Because it allows the measurement of a spectrum for each pixel of an image, it overcomes the issue concerning the spatial definition. Hence, the identification of the components in a urinary stone with a fully analyst-independent method was possible. In that work, urinary stones could be classified into groups according to their chemical composition and stone structure, as previously described in Refs. 10 and 20, and the results were compared with those obtained from optical microscopy. However, the results achieved were not directly comparable to those coming from IR spectroscopy, because the classification of the stones did not include the quantification or approximate gradation of the chemical components. A new study involving the reference and most commonly used method for the classification of urinary stones, IR spectroscopy, seems of high interest to test the capability of this methodology for use in routine analysis. This work describes the potential of the developed near-infrared (NIR) HSI methodology for the automatized analysis of urinary stones. It combines data analysis steps already described in the literature, but focuses on a new application that represents a clear advantage against the state of the art in clinical laboratories.

The novelties of the work presented here are (1) to present a novel methodology for the classification of urinary stones, based on HSI, and giving pixel-to-pixel classification results; (2) comparing the performance of the newly designed methodology with the reference technique, IR spectroscopy; (3) using a high-resolution technique while keeping a high analysis speed; and (4) posing the bases for the consideration of this methodology, which is fast, inexpensive, and analyst independent, as an alternative to the reference technique.

2 Materials and Methods

2.1 Samples

A total of 200 samples of urinary stones were selected from a library of more than 1400 units. The urinary stones were obtained either from natural expulsion or surgical removal from patients of the urology service at the Hospital Universitari de Bellvitge, Barcelona (Spain). The samples underwent no other treatment than ethanol and water rinsing for cleaning and convenient drying for their proper conservation. Note that in this work, sample stands for a urinary stone (or various stones or stone fragments) collected from a patient in a single episode. If a sample consists of several pieces coming from the cleavage of the stone, they are not considered independent. Any piece of stone obtained directly from the patient (e.g., after a lithotripsy treatment) or after cutting the stone for its analysis is considered a fragment.

The selection criterion was to include the widest variability within each class of stones in terms of structure and composition considering both pure and mixed components. For the analysis of the samples used to compare both methodologies, a few representative fragments were used from each stone sample. The methodology is intended to prove its efficacy for the analysis of some fragments instead of selecting all the pieces. The

fragments were chosen so that they were representative for the structure of the whole stone (core components, surface deposits, etc.).

The sample preparation differs for each of the analysis techniques used in this work. Stone samples were selected using microscopy as described in Sec. 2.2 and later analyzed using IR (Sec. 2.3) and NIR-HSI (Sec. 2.4). Note that NIR-HSI measurements were performed first because HSI is a nondestructive technique.

Microscopy only required cutting the samples for the observation of the outer and inner parts of the stone.

For the measurement of the IR spectra of the samples, a representative fragment of each sample was dried in an oven for 24 h at 40°C prior to the analysis. The sample was ground in an Agatha mortar and 0.9 mg of the sample was then mixed with 0.3 g of KBr powder. A pellet was prepared by setting this mixture under 10 Tm pressure in a manual press (Perkin Elmer, MA, USA).

Different from IR, HSI is fundamentally a surface analysis technique and requires a relatively flat surface for the measurements. Reflectance spectra are measured, so an uneven surface would lead to an important signal loss. All samples were cut with a surgical knife, thus fulfilling the requirements of HSI and allowing the acquisition of spectra from the inner part of the stones, which usually carry important information related to the stone history. Due to the characteristics of the technique, the whole exposed surface was analyzed after placing the sample on a plastic holder with the area of interest facing the detector. For those samples in which the inner and outer parts were clearly different, both were analyzed for better accuracy of the result.

2.2 Microscopy

Stereoscopic microscopy was used for the selection of samples (training and test sets) prior to the IR and NIR-HSI measurements, according to morphological features such as texture, color, and structure. These features allow the achievement of the sample selection criteria indicated in Sec. 2.1. Microscopy analyses were performed as widely described in Refs. 10 and 11.

For those samples not clearly classified using optical microscopy, scanning electron microscopy was used since it allowed the close visualization of the structure of the stones and the performance of elemental analysis. The equipment used was a JEOL JSM-6300 scanning electron microscope (Japan), coupled to an Oxford Instruments Link ISIS-200 x-ray dispersive energy spectrometer (UK).

Microscopy should be considered in this work as a support methodology used for sample selection, because it only gives qualitative information. The numerical comparison between IR and NIR-HSI was done on all the samples and standards after this selection step.

2.3 IR Methodology

IR spectroscopy has been used as reference methodology to test the results of NIR-HSI. The main advantages of considering IR as the standard are the robustness and wide acceptance of the technique and the calculation of a numerical value for the sample composition. The IR spectra of the prepared pellets were collected using an IR spectrometer Spectrum BX (Perkin Elmer, MA, USA). The spectral range measured ran from 450 to 4400 cm^{-1} (which corresponds to a wavelength range from ~2200 to 22,000 nm), with a spectral resolution of 4 cm^{-1} .

For the determination of the sample composition, a comparison of the measured spectra with those in Ref. 21 was done. This collection of spectra considered pure compounds, combination of two species, and even combinations of three components for the common cases of calcium oxalate mono and dihydrate and carbonate apatite, including different gradations for the amounts of each component in a 10% (w/w) grading.

2.4 NIR-HSI Device and Architecture Setup

HSI technique, also known as chemical imaging, can be regarded as the stacking of pictures of the same surface, each of them taken at a different wavelength.²² This group of images defines the so-called hypercube, a three-dimensional dataset that is analyzed as a single image containing a full spectrum for each pixel.²³ This technique, therefore, leads to the complete characterization of every pixel of the image. Compared to IR, HSI offers not only one spectrum per sample, but several hundreds while consuming the same amount of time (a few seconds) for the measurements.

The HSI device used was configured at DICMA, Sapienza–Università di Roma (Rome, Italy) and is precisely described in the previous work.¹⁹ The main feature of the equipment is an imaging spectrometer ImSpector™ N17E (Specim, Finland) with a spatial resolution $<15 \mu\text{m}$. The spectral resolution was 7 nm, covering the spectral range from 1000 to 1700 nm, which yielded a total of 121 wavelengths (data points/spectrum) measured. The spectrometer was coupled to a 50 mm lens with an image resolution of 320 pixels. The software Spectral Scanner™ v.2.3 (DV Optics srl, Italy) was used for the acquisition, preprocessing, and visualization of the images. The reflectance signal was calculated as a function of the calibrated black and white limits.

It is interesting to note that both IR and NIR are included within the IR spectral range but they do not overlap. The equipment used for those measurements, therefore, gives spectrally independent signals. This fact makes it clear that the chemical properties (i.e., bond vibrations or rotations) observed for the classification are different for each case. NIR represents an alternative spectroscopic approach, which offers results comparable to IR, yet requires little sample pretreatment.

When using HSI, the radiation penetration depth is defined as the depth at which the incident light is reduced by 99%. It varies, in fact, according to sample characteristics, surface attributes, and investigated wavelengths (depth is lower when wavelength increases). In this study, this magnitude can be estimated as 10 to 20 μm .

The pixel resolution is much smaller than the size of any urinary stone (which generally ranges from a few millimeters to 2 cm), and is also smaller than most surface imperfections or porosity. This resolution prevents any remarkable signal loss or pixel misclassification, because the area surrounding the surface defect would still be correctly classified.

2.5 Data Analysis

The data treatment included the handling of the spectra, creation of the classification (reference) model, and sample treatment.

The NIR reflectance spectra were directly analyzed as obtained, i.e., no derivatives or other data pretreatment were applied. However, due to the large amount of information available from the HSI measurements, the reduction of the dimensionality of the system was required so that only the most

influential variables (wavelengths) were taken into consideration. For this issue, a randomized principal component analysis (PCA) algorithm was used to select the 10 principal components, a figure chosen by cross-validation. This way each pixel is represented by a vector of 10 components instead of more than 100 spectral measurements. This decreases the number of parameters for the classifier to learn, thus preventing overfitting to a great extent. Since the variables that had little classification power were not included in the model, the noise of the system was likewise decreased.²⁴

The classification model included a variable number between six and eight stone fragments of each stone type with homogeneous composition. Each stone fragment was collected from a different patient, so model overfitting was reduced. Note that although only a few samples were taken in the training set according to the characteristics of the HSI technique (i.e., acquisition of a spectrum for each pixel of the image sample), thousands of pixels were used for training purposes. The number of samples in the model was large enough to cover all the naturally occurring components in urinary stones.

The image analysis of the training and test sample sets was performed using SciPy and Scikit-learn, two open source Python libraries for scientific analysis.^{25,26}

A series of classifiers were tested for the creation of a model able to categorize the samples. A classifier is any mathematical function able to assign a label “class” to a given sample when it has been learned on a specific training set.²⁷ Following the criteria of the best classification rate, quadratic discriminant analysis (QDA) was selected. This classifier is a classic Bayesian method, generally used on machine learning. It assumes the normal distribution of the data within each class and different covariances within classes.²⁸ Due to the complex nature of the sample set used in this work, QDA is a good approach since it can establish boundaries between classes based on quadratic algorithms, so it is more flexible than linear classifiers. This classification scheme showed a better performance than others tested, including k-nearest neighbor, random forest, and support vector machines.

The creation of the model included a test step using the leave-one-out approach. The vectors of 10 principal components of every pixel of each fragment are placed in a pool. Then, each time a certain fragment has to be analyzed, that is when we want to assign a class label to each of its pixels, they are removed from the pool which now is the training set. The QDA classifier parameters are learned and the classification on the given fragment vectors, which act as the testing set, is performed. This process is iterated for every fragment. In pattern classification literature, this procedure is known as leave-one-out, although in this case it was done at a fragment level.²⁴

When the classification model created using the standards was applied to the samples, the structural analysis of the stone was achieved. The physical structure of the stone was reconstructed based on the results for the analysis of each pixel. These procedures lead to the creation of chemical maps of the stones which represent the spatial resolution of the technique.

3 Results and Discussion

3.1 Performance of the HSI-NIR Model

The training set was analyzed using IR spectroscopy (reference values) and also using NIR-HSI. In this case, only homogeneous samples were considered, since the objective of this step was to

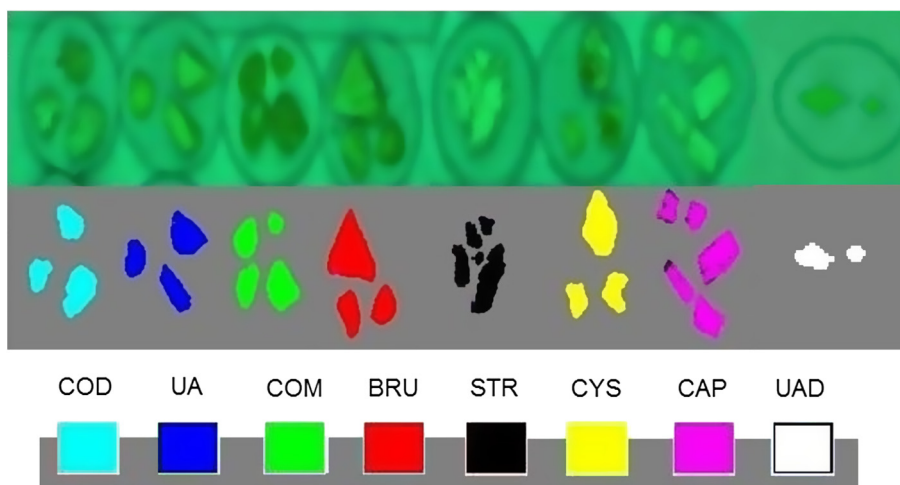


Fig. 1 Results for the classification using the training set. Not all the samples used for the creation of the model are shown. Upper row: reconstructed image from the original stones, obtained from the Spectral Scanner software. The different fragments (with different origins) can be appreciated. Lower row: results of the classification model, where each pixel is assigned a class and, so, a different color (from MATLAB® software).

train the classifier in the recognition of stone classes using a large number of pure pixels. It was easier to isolate pure pixels in homogeneous stones. The advantages in spatial resolution of HSI are not relevant in this step. The graphical results obtained for the HSI model performance are shown in Fig. 1.

The overall correct classification rate of the model was calculated to be 90.4% in terms of correctly classified pixels compared to the results obtained by IR spectroscopy. The specific efficacy of the model on the classification of each stone type is shown in the normalized confusion matrix (Table 1). The diagonal of the matrix shows how, for most classes, only a minor number of pixels are confused with other classes, with the exception of carbonate apatite $[\text{Ca}_{10}(\text{PO}_4)(\text{CO}_3, \text{OH})_6(\text{OH})_2]$ (CAP) and struvite ($\text{Mg} \cdot \text{NH}_4\text{PO}_4 \cdot 6\text{H}_2\text{O}$) (STR). Indeed, the confused pixels for the rest of the stone classes represent only residual values. Note the composition difference

between CAP and hydroxylapatite (lacking any carbonate ion in the lattice), sometimes misclassified as the main component of CAP stones.

It can be appreciated that the general behavior of the model is very efficient, with the overall results >95% of correct prediction for most stone classes. The exception is represented by CAP and STR, which are confused with each other in an important percentage (30 to 40%). These results can be attributed to the similar features their NIR spectra share and the related appearance of both types of urinary stones. The model shows a good general result, even considering the remarkable variability within groups seen in the spectra, as plotted in Fig. 2. The general trend of the spectra in each class and the unique spectral bands for some components lead to a proper classification result. The mean spectra of the training set shows such specific bands (see Fig. 2). As specified in Sec. 2.4, NIR does not overlap with

Table 1 Normalized confusion matrix. The efficiency of the model can be measured as a percentage of correct classification for each stone class.

Type of stone (mineralogical composition)	Predicted values (%)							
	BRU	COM	UA	COD	CAP	CYS	STR	UAD
BRU	99.37	0	0.08	0.55	0	0	0	0
COM	0.04	99.75	0	0.04	0	0.17	0	0
UA	0	0	99.33	0	0.16	0.08	0	0.43
COD	0	0	0	99.77	0.17	0	0.06	0
CAP	4.83	0	0	1.26	73.33	0.07	20.51	0
CYS	0	0	0	0.03	0	99.84	0.13	0
STR	0	0	0	0	26.55	0.02	73.43	0
UAD	2.06	0	0.36	4.58	0	0.72	1.17	91.11

BRU, brushite ($\text{CaHPO}_4 \cdot 2\text{H}_2\text{O}$); COM, calcium oxalate monohydrate ($\text{CaC}_2\text{O}_4 \cdot \text{H}_2\text{O}$); UA, uric acid ($\text{C}_5\text{H}_4\text{N}_4\text{O}_3$); COD, calcium oxalate dihydrate ($\text{CaC}_2\text{O}_4 \cdot 2\text{H}_2\text{O}$); CAP, carbonate apatite $[\text{Ca}_{10}(\text{PO}_4)(\text{CO}_3, \text{OH})_6(\text{OH})_2]$; CYS, cystine ($\text{C}_6\text{H}_{12}\text{N}_2\text{O}_4\text{S}_2$); STR, struvite ($\text{Mg} \cdot \text{NH}_4\text{PO}_4 \cdot 6\text{H}_2\text{O}$); UAD, uric acid dihydrate ($\text{C}_5\text{H}_4\text{N}_4\text{O}_3 \cdot 2\text{H}_2\text{O}$).

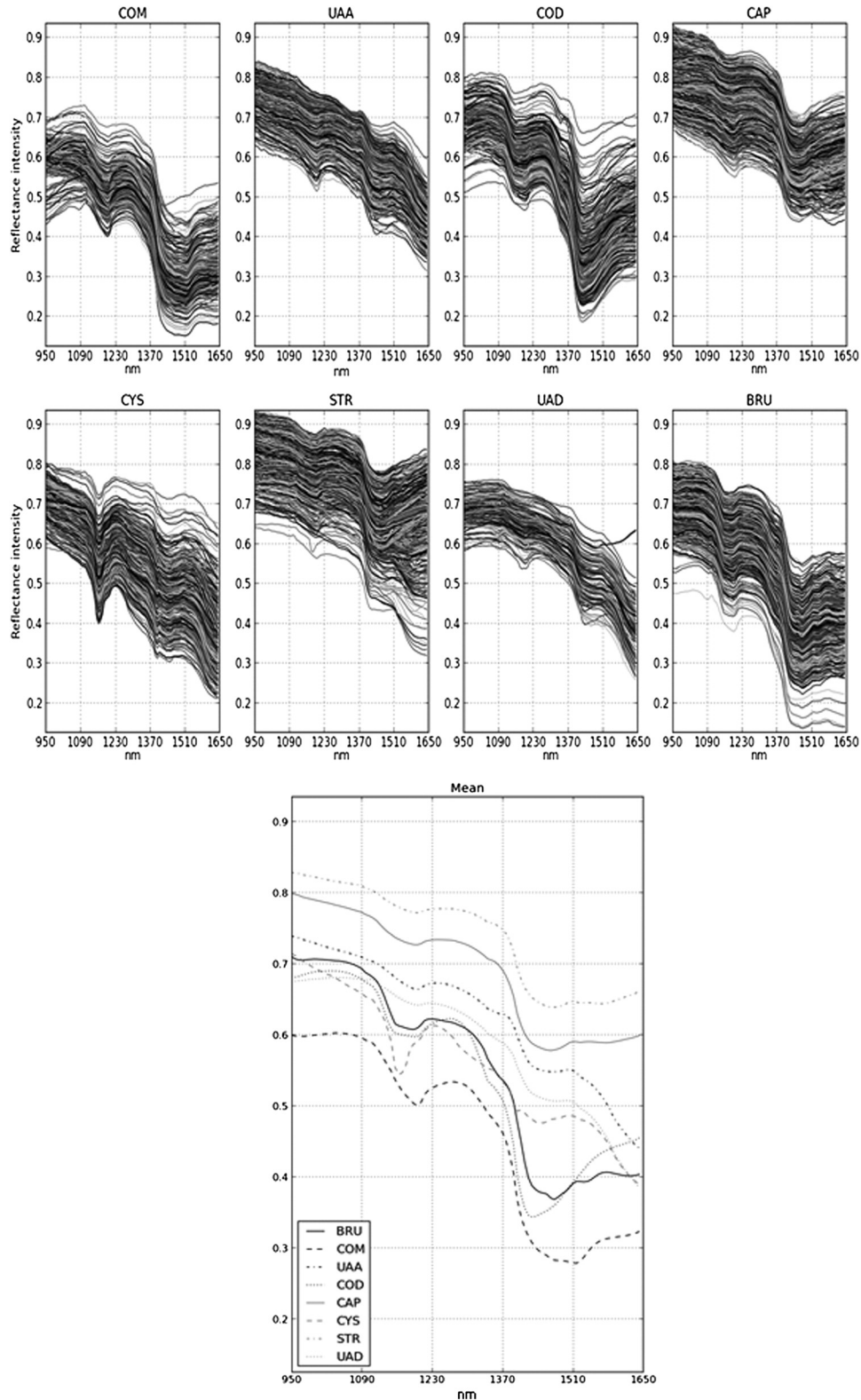


Fig. 2 First and second rows: accumulation of all the spectra of the training set, plotted as reflectance intensity versus wavelength (nm). The mean spectra are plotted at the bottom of the image.

the IR spectral range. Despite this important difference, most of the relevant bonds in organic components can be identified in the NIR range, including: C–H, S–H, N–H, O–H, or O–H linked to an aromatic ring. The sensitivity of those bonds (which are also identified in IR spectroscopy) in the NIR range allows

for proper recognition of urinary stones' mineralogical components, as discussed here.

The distribution of pixels (depending on the size and number of pixels used in the model) of each class used for creating the model is shown in Fig. 3. Only uric acid dihydrate

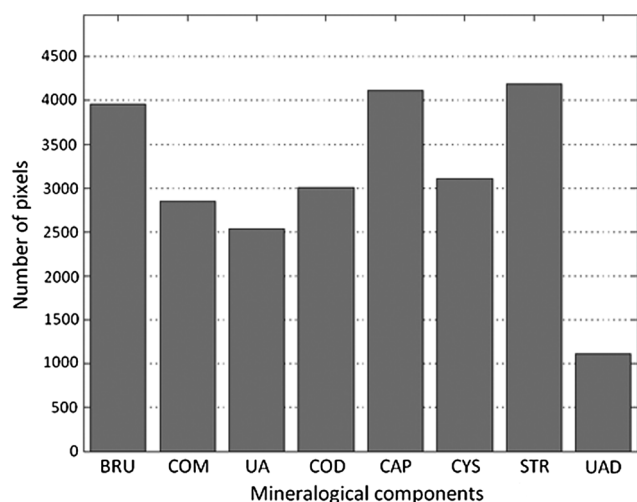


Fig. 3 Frequencies histogram. The model is created from such a distribution of pixels. The total count of pixels is related not only to the number of fragments considered for each group but also to the size of those fragments.

($C_5H_4N_4O_3 \cdot 2H_2O$) (UAD) counts had a smaller number of pixels for the creation of the model; it was difficult to find stones rather pure in UAD and with no contamination of uric acid ($C_5H_4N_4O_3$) (UA), since UAD rapidly transforms into UA in contact with urine.²⁹ The computer model, though, is able to perfectly discriminate (>99%, as seen in Table 1) between the two derivatives of uric acid, and also to distinguish them from any other component to a great extent.

3.2 Conventional IR Analysis of Samples

From the test samples group, only one sample was discarded from the experiment using IR spectroscopy. Its composition, according to the IR analysis, was 100% dittmarite, corresponding to the chemical composition $MgNH_4PO_4 \cdot H_2O$. This mineral corresponds to the dehydration of STR, the hexahydrated derivative, which may take place during storage periods of these stones.³⁰ The NIR-HSI test set did not include such unexpected minerals as standards, so the sample was not considered.

3.3 Implementation of the NIR-HSI Model

The created model was rapidly implemented on the 200 test samples by using the described data analysis software. Two types of output were demanded from this software: the classification of each pixel into a group from the standards and a reconstructed picture of the stone, from which the location of all components and their spatial relationships are easily recognizable. These pictures represent the spatial resolution, that is, the possibility of performing a topological assessment

Table 2 Overview of the classification results obtained by the near-infrared hyperspectral imaging (NIR-HSI) methodology and their correlation to IR spectroscopy for each type of stone. Results correspond to a total of 200 urinary stone analyses using both techniques.

Type of stone	BRU	CAP	COD	COM	CYS	STR	UA	UAD	Mixed
Correlation (%)	88	60	78	94	100	64	93	90	78

of the detected species in the sample offered by this methodology: the added value that NIR-HSI offers compared to IR spectroscopy.

The samples in the test set were analyzed using the NIR-HSI model and the results, expressed as percentage for each component, were compared to the composition measured by IR spectroscopy. Assuming an error <10% for the IR classification due to the component gradations in the consulted bibliography, the results from NIR-HSI were considered to correlate with the IR results if the NIR-HSI composition matched, considering $\pm 10\%$ deviation.

A thorough analysis of the results shows the composition obtained by NIR-HSI to generally fit that from IR (achieving 70% correlation), with some variations that require a more careful analysis. It should be taken into account that the sensitivity of minor components is higher for the NIR-HSI technique than for IR spectroscopy. Minor components could cause only a small IR spectral band to grow or appear, so the spectrum would hardly be changed. IR spectroscopy strongly relies on the analyst's experience, so such small changes might be hard to quantify. Instead, since each pixel is analyzed individually by NIR-HSI, minor components are identified with the same precision as main constituents of the sample. Therefore, as will be seen later, NIR-HSI can give more information in some cases than IR spectroscopy does.

The description of the classification results and their correlation to the IR analyses is listed as groups based on their mineralogical composition and is summarized in Table 2.

3.3.1 Calcium oxalate

This complex group of urinary stones includes calcium oxalate monohydrate ($CaC_2O_4 \cdot H_2O$) (COM), calcium oxalate dihydrate ($CaC_2O_4 \cdot 2H_2O$) (COD) and, frequently, a mixture of those components together with CAP. In addition, COD is not stable in contact with urine, so it slowly transforms into the thermodynamically most stable derivative COM.³¹ Thus, both species can be found in a wide range of proportions. When the model was applied to this group of samples, the classification for those containing basically COM correlated >90% with that of IR spectroscopy. For COD and mixed stones, the percentage stayed close to 80%. This difference could be based on terms of frequency and composition. While stones whose composition is >90% COM are very common, COD tends to be mixed with COM (often formed from COD transformation) or CAP in variable amounts.¹⁰ This fact could cause the calculated composition by NIR-HSI to be outside of the $\pm 10\%$ error for the IR spectroscopy results, thus a wrong correlation was considered. It must be stressed that NIR-HSI is able to locate the different components in the stone, allowing the performance of a full textural characterization of the minerals constituting the stone itself. Starting from these features, it is possible to derive useful information about stone formation and, as a consequence, to formulate a description of the position and the moment in which each component precipitated. Thus, these mixtures of several components were described in a further dimension.

3.3.2 Cystine

This stone type presented the highest correlation rate, namely 100% of the samples analyzed by NIR-HSI completely agreed with the IR analysis. This type of stone is strictly related to a genetic disorder, so cystine ($C_6H_{12}N_2O_4S_2$) (CYS) precipitates

in special conditions and it usually does not coprecipitate. Besides, since CYS is the only species in the studied group containing C–H bonds, its NIR spectrum shows unique features.

3.3.3 Phosphate stones

CAP and STR stones, as well as the less frequent brushite ($\text{CaHPO}_4 \cdot 2\text{H}_2\text{O}$) (BRU) group form this heterogeneous group of stones. The classification of BRU urinary stones by NIR-HSI correlated as much as 87.5% to that from IR spectroscopy. Only a few pixels in several samples were confused with CAP (as seen in the model), which is also a calcium phosphate. In regard to CAP and STR, the NIR-HSI model could match ~60 to 65% (see Table 1) of the results to those obtained by IR spectroscopy. As seen in Fig. 2, the NIR spectra of both species are similar and they tend to precipitate together, so the quantification of each component in mixed stones becomes difficult. Although the composition obtained by NIR-HSI was not dramatically different from the IR results (most samples remained within the $\pm 20\%$ range), the portion of samples that were outside the $\pm 10\%$ region set as the correlation range was higher than that of other urinary stone groups.

3.3.4 Uric acid

This type of stone actually includes two different components: UA and its kinetic derivative, the dihydrated form (UAD). The analysis of both components by NIR-HSI yielded very good results, with a correlation $>90\%$. The model could distinguish with little error these two forms of UA, and its comparison to the IR results were correct.

3.4 Spatially Defined Analysis

As already stated, the main advantage of the NIR-HSI technique over the conventional IR spectroscopy is the spatial resolution of the analysis (i.e., topological assessment of the different mineralogical species), not available when the sample is ground for the IR measurements. Thus, NIR-HSI offers the possibility to describe all the stages in the stone formation and the urine

conditions at each point of the process, information that can direct a treatment that is precisely adapted to every patient. This is the advantage that the examples presented in this section highlight.

Among the total amount of samples that were analyzed, some specific representative examples will be accurately described in order to illustrate the performance of the developed model and to highlight the differential results that both techniques offer (Fig. 4). The results for the composition of these examples are listed in Table 3.

The first example [Fig. 4(a)] shows a calcium oxalate mixed stone, with a similar composition for both methodologies. This stone presents a singular structure: it is basically a COM stone, totally covered by a COD layer. Thus, the order of precipitation is important; COD (which usually precipitates due to a high concentration of Ca ion and oxalate in urine³²) precipitated exclusively at the end of the stone episode. In this case, it should be appreciated that the higher percentage of COD quantified by the NIR-HSI technique is due to the analysis of both the inner part and surface at the same time so the COD surface is bigger than that for COM. HSI is a surface technique, so attention shall be paid to which part of the stone is being analyzed. Once this is clear, HSI allows the description of two steps in the stone formation, while IR can only give a general composition ratio of these two phases.

The stone in Fig. 4(b) corresponds to a very common composition, calcium oxalate and CAP. In this case, the stone was formed as COD and the core transformed into COM due to the higher stability of the latter.¹⁰ We can observe this phenomenon as a different color in the stone nucleus. CAP did precipitate in this stone as a few deposits within the stone structure. Both techniques could identify the same three components; the higher percentage of COM in the IR should be attributed to the difference of relative surface (NIR-HSI) and relative weight in the stone (IR) of this component. NIR-HSI allows the location of CAP not only in the stone core so the stone formation steps become clearer when image analysis is used.

The mixed stone of UA and COM in Fig. 4(c) yielded a very similar percentage composition when analyzed by the two

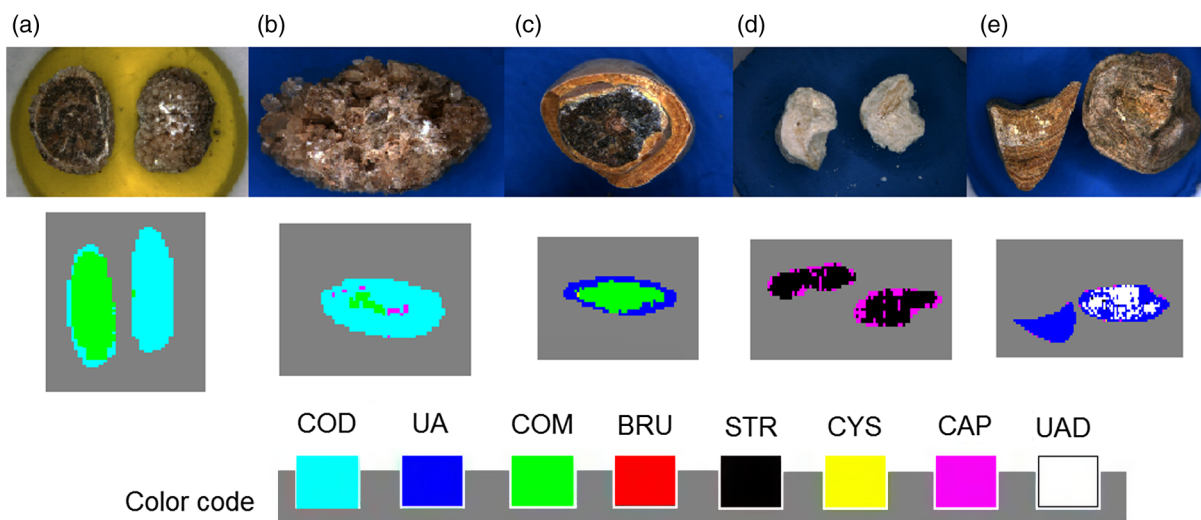


Fig. 4 Examples of some results for stone analysis comparing near-infrared hyperspectral imaging and infrared spectroscopy. First row: color, real pictures of the samples. Second row: reconstructed images corresponding to the samples listed in the first row; these images are the output of the imaging analysis software used (the legend shows the correspondence between colors and components).

Table 3 Mineralogical composition corresponding to the samples listed in Fig. 4, according to the two methodologies used. The composition values are expressed as percentage.

Sample	a	b	c	d	e
NIR-HSI		90 COD			
	40 COM		78 COM	63 STR	55 UA
		5 COM			
	60 COD		22 UA	37 CAP	45 UAD
		5 CAP			
IR		80 COD	80 COM	70 STR	60 UA
	60 COD				
		15 COM	20 UA	30 CAP	40 UAD
	40 COM				
		5 CAP			

methodologies suggested in this work. However, NIR-HSI allowed the location of COM in the core of the stone, so the acidic urine conditions needed for the precipitation of UA can be located in the latter stages of the stone formation. This separate analysis of core and shell parts requires the addition of steps to the stone analysis process by IR spectroscopy (the measurement of two spectra), so the time for the analysis is increased.

The stone in Fig. 4(d) is a common mixed stone, which includes CAP and STR. These stones usually lack any defined structure, and this exact situation can be seen in the picture. The quantification of the stone components is really similar using both techniques.

In Fig. 4(e), UAD is the kinetic derivative of UA, and, as seen in the calcium oxalate case, it also slowly transforms into the most stable UA if it remains in contact with urine.²⁴ While the composition according to both techniques is basically the same, HSI also gives the distribution of components, which appears to be different in the two analyzed fragments. HSI is able, in this case, to define which fragments are UAD, so the description of the sample is totally precise for this particular patient.

4 Conclusions

The present work has verified for the first time the modern methodology (NIR-HSI) applied to urinary stone analysis by a comparison with the conventional procedure based on IR spectroscopy. The developed HSI methodology presents a unique distinctiveness against conventional IR spectroscopy for urinary stones classification, by appropriately locating components in the stone. Given the relevance of the location of components in the stone structure for the proper description of the etiologic causes, this methodology represents a clear advantage compared to IR in terms of performance.

The efficiency of the software turns this technique into a totally analyst-independent procedure that requires a very short analysis time, typically 1 to 2 min including spectra

acquisition and data analysis. This time is comparable to IR spectroscopy, in the case where IR is linked to ATR, which shortens the sample preparation time described in this publication (there is no need to prepare pellets). Maintenance costs are as low as in IR and no chemicals are needed for the analysis. The versatility of HSI for the analysis of solid samples (not very extended in clinical laboratories) provides interesting possibilities to easily adapt the device to other sample types and medical specialties. This versatility would compensate the initial investment required in any laboratory for an HSI device. These advantages position this methodology as an attractive update for stone analysis in clinical laboratories.

The high performance of the developed technique leads to a more accurate description of the stone history, which, in turn, allows a more precise diagnosis. NIR-HSI produces key information for an individualized treatment.

Acknowledgments

The authors acknowledge the financial support of the Spanish Ministerio de Economía y Competitividad (MINECO, Spanish Ministry for Economy and Competitiveness) through the CTM2012-30970 Project and the Ministerio de Educación, through Becas FPU (Ref. AP2009-3245) and the Subprogram Estancias Breves (EST2012-940), for funding F. Blanco stages in foreign institutions. The Spanish-Italian Program for Integrated Action is likewise acknowledged (Ref. IT2009-0024). Second and third authors were supported by Spanish R&D projects TIN2011-29494-C03-02 and TRA2011-29454-C03-01, respectively.

References

1. A. Hesse et al., "Study on the prevalence and incidence of urolithiasis in Germany comparing the years 1979 vs. 2000," *Eur. Urol.* **44**, 709–713 (2003).
2. C. D. Scales et al., "Prevalence of kidney stones in the United States," *Eur. Urol.* **62**, 160–165 (2012).
3. H. G. Tiselius, "Who forms stones and why?," *Eur. Urol. Suppl.* **10**, 408–414 (2011).
4. A. Hesse et al., *Urinary Stones: Diagnosis, Treatment and Prevention of Recurrence*, 1st ed., Karger, Basel (2009).
5. R. Siener and A. Hesse, "Comparative costs of various treatment strategies and preventive measures," in *Urolithiasis: Basic Science and Clinical Practice*, J. J. Talati et al., Eds., pp. 897–901, Springer, Amsterdam (2013).
6. C. Y. C. Pak et al., "Predictive value of kidney stone composition in the detection of metabolic abnormalities," *Am. J. Med.* **115**, 26–32 (2003).
7. G. Rebenitsch et al., "Assessment and maintenance of the quality of urolith analyses in a comparison of methods. 4th International Ring Test to check quality," *Int. Urol. Nephrol.* **20**(1), 35–45 (1988).
8. J. L. García, M. J. Torrejón, and M. Arroyo, "Development of a method for the quantitative analysis of urinary stones, formed by a mixture of two components, using infrared spectroscopy," *Clin. Biochem. Acta A* **93**, 582–587 (2012).
9. R. Selvaraju, G. Thirupathi, and A. Raja, "FT-IR spectral studies on certain human urinary stones in the patients of rural area," *Spectrochim. Acta A* **93**, 260–265 (2012).
10. F. Grases et al., "Simple classification of renal calculi closely related to their micromorphology and etiology," *Clin. Chim. Acta* **322**, 29–36 (2002).
11. M. Daudon, C. A. Bader, and P. Jungers, "Urinary calculi: review of classification methods and correlations with etiology," *Scanning Microsc.* **73**(3), 1081–1104 (1993).
12. D. B. Leusmann, "A classification of urinary calculi with respect to their composition and micromorphology," *Scand. J. Urol. Nephrol.* **25**, 141–150 (1991).

13. F. Blanco et al., "High precision mapping of kidney stones using μ -IR spectroscopy to determine urinary lithogenesis," *J. Biophotonics* **1–9** (2014).
14. F. L. Coe, A. Evan, and E. Worcester, "Kidney stone disease," *J. Clin. Invest.* **115**(10), 2598–2608 (2005).
15. G. Lu and B. Fei, "Medical hyperspectral imaging: a review," *J. Biomed. Opt.* **19**(1), 010901 (2014).
16. J. R. Duann et al., "Separating spectral mixtures in hyperspectral image data using independent component analysis: validation with oral cancer tissue sections," *J. Biomed. Opt.* **18**(12), 126005 (2013).
17. M. Pucetaite et al., "Application of infrared spectroscopic imaging in specular reflection mode for determination of distribution of chemical components in urinary stones," *J. Mol. Struct.* **1031**, 38–42 (2013).
18. S. Piqueras et al., "Resolution and segmentation of hyperspectral biomedical images by multivariate curve resolution-alternating least squares," *Anal. Chim. Acta* **705**, 182–192 (2011).
19. F. Blanco et al., "Hyperspectral imaging based method for fast characterization of kidney stone types," *J. Biomed. Opt.* **17**(7), 076027 (2012).
20. G. Schubert, "Stone analysis," *Urol. Res.* **34**, 146–150 (2006).
21. A. Hesse and G. Sanders, *Atlas of Infrared Spectra for the Analysis of Urinary Concrements*, 1st ed., Georg Thieme Verlag, Stuttgart (1988).
22. C. Gendrin, Y. Roggo, and C. Colelt, "Pharmaceutical applications of vibrational chemical imaging and chemometrics: a review," *J. Pharm. Biomed. Anal.* **48**, 533–553 (2008).
23. G. Reich, "Near-infrared spectroscopy and imaging: basic principles and pharmaceutical applications," *Adv. Drug Deliv. Rev.* **57**, 1109–1143 (2005).
24. R. G. Brereton, *Applied Chemometrics for Scientists*, 1st ed., Wiley, New Jersey (2007).
25. SciPy, "SciPy.org," 05/11/2014, <http://www.scipy.org/> (13 November 2014).
26. Scikit-Learn, "Machine learning in Python," 07/11/2014, <http://scikit-learn.org/> (13 November 2014).
27. L. I. Kuncheva, *Combining Pattern Classifiers. Methods and Algorithms*, 1st ed., Wiley, New Jersey (2004).
28. T. Hastie, R. Tibshirani, and J. Friedman, *The Elements of Statistical Learning: Data Mining, Inference and Prediction*, 2nd ed., Springer, New York (2009).
29. F. Grases et al., "Uric acid calculi: types, etiology and mechanisms of formation," *Clin. Chim. Acta* **302**, 89–104 (2000).
30. A. Hesse and D. Heimbach, "Causes of phosphate stone formation and the importance of metaphylaxis by urinary acidification: a review," *World J. Urol.* **17**, 308–315 (1999).
31. D. Skrtic and H. Furedi-Milhofer, "Precipitation of calcium oxalates from high ionic strength solutions. V. The influence of precipitation conditions and some additives on the nucleating phase," *J. Cryst. Growth* **80**(1), 113–120 (1987).
32. J. R. Asplin et al., "Metabolic urinary correlates of calcium oxalate dihydrate in renal stones," *J. Urol.* **159**, 664–668 (1998).

Francisco Blanco received a PhD degree in chemistry from Universitat Autònoma de Barcelona (Spain). This degree, developed in the Centre GTS–Chemistry Department at the same university, has its main focus on the analysis of urinary lithiasis. He has developed several works on kidney stone classification and the study of promoters and inhibitors of the stone formation process, using a number of chromatographic, spectroscopic, and chemical speciation techniques.

Felipe Lumbreras received a PhD degree in computer science from Universitat Autònoma de Barcelona (UAB), Barcelona, Spain, in 2001. He is currently an associate professor with the Department of Computer Science, UAB, and he also is a member of the Computer Vision Center, UAB. His research interests include texture analysis, 3-D reconstruction, and computer vision for automotive applications.

Joan Serrat is an associate professor at the Computer Science Department of the Universitat Autònoma de Barcelona and also a member of the Computer Vision Center. His current research interest is the application of probabilistic graphical models to computer vision problems such as feature matching, tracking, and video alignment. He has coauthored more than 40 papers and four patents, and has been head of several computer vision projects for industries.

Roswitha Siener is a professor in the Department of Urology, University of Bonn, Germany, and head of the University Stone Centre. Her scientific focus includes all aspects of urinary stone disease.

Silvia Serranti is an assistant professor in the Department of Chemical Engineering, Materials and Environment (DICMA), Faculty of Civil and Industrial Engineering, University of Rome "La Sapienza." His research activity is related to the field of primary and secondary raw materials characterization and valorization, and is documented by more than 120 scientific papers published in international journals and in proceedings of international conferences and by the participation in 11 research projects financed by the European Union.

Giuseppe Bonifazi is a full professor of raw materials beneficiation at La Sapienza–University of Rome. He has an extensive experience over 30 years on characterization of particulate solids, specifically with reference to the development and setup of procedures for objects and material identification, both at laboratory and industrial scales, using pattern recognition techniques based on classical and hyperspectral imaging-based techniques.

Montserrat López-Mesas has received a PhD degree in chemistry and a postdoctor at Stanford University. At present, he is a lecturer professor at UAB. His research interests include analysis of organic, inorganic, and emerging contaminants in several matrices, such as water and solids, characterization of inhibitors and promoters of urolithiasis in urine, and development of new methodologies for the classification of kidney stones. He has participated in several EU-FP7 projects and national projects and published more than 25 papers and 3 patents.

Manuel Valiente has received a PhD degree in analytical chemistry and inorganic chemistry. He is a full professor in analytical chemistry at the Universitat Autònoma de Barcelona. He has published 188 papers in international refereed journals, eight patents, and has been the supervisor of 29 PhD theses and 34 graduate theses. He is coordinator of six EU projects. He is a specialist in environmental monitoring and remediation technologies and an expert in the application of advanced characterization and speciation techniques in the analysis of biomaterials.